LJMU Research Online

Shipp, N, Riley, AH, Simpson, CM, Bieri, R, Necib, L, Arora, A, Fragkoudi, F, Gómez, FA, Grand, RJJ and Marinacci, F

 Auriga Streams II: orbital properties of tidally disrupting satellites of Milky Way-mass galaxies

https://researchonline.ljmu.ac.uk/id/eprint/27308/

Article

For more information please contact researchonline@ljmu.ac.uk

Auriga Streams II: orbital properties of tidally disrupting satellites of Milky Way-mass galaxies

Nora Shipp [ORCID],[1]★ Alexander H. Riley [ORCID],[2] Christine M. Simpson [ORCID],[3] Rebekka Bieri [ORCID],[4] Lina Necib [ORCID],[5] Arpit Arora,[1] Francesca Fragkoudi [ORCID],[2] Facundo A. Gómez [ORCID],[6] Robert J. J. Grand [ORCID][7] and Federico Marinacci [ORCID][8,9]

[1]*Department of Astronomy, University of Washington, Seattle, WA 98195, USA*

[2]*Institute for Computational Cosmology, Department of Physics, Durham University, South Road, Durham DH1 3LE, UK*

[3]*Argonne Leadership Computing Facility, Argonne National Laboratory, Lemont, IL 60439, USA*

[4]*Department of Astrophysics, University of Zurich, CH-8057 Zurich, Switzerland*

[5]*Department of Physics and Kavli Institute for Astrophysics and Space Research, Massachusetts Institute of Technology, 77 Massachusetts Ave, Cambridge, MA 02139, USA*

[6]*Departamento de Astronomía, Universidad de La Serena, Av. Juan Cisternas 1200 Norte, La Serena, Chile*

[7]*Astrophysics Research Institute, Liverpool John Moores University, 146 Brownlow Hill, Liverpool L3 5RF, UK*

[8]*Department of Physics and Astronomy 'Augusto Righi', University of Bologna, Via Gobetti 93/2, I-40129 Bologna, Italy*

[9]*INAF, Astrophysics and Space Science Observatory Bologna, Via P. Gobetti 93/3, I-40129 Bologna, Italy*

ABSTRACT

Galaxies like the Milky Way are surrounded by complex populations of satellites at all stages of tidal disruption. In this paper, we present a dynamical study of the disrupting satellite galaxies in the Auriga simulations that are orbiting 28 distinct Milky Way-mass hosts across three resolutions. We find that the satellite galaxy populations are highly disrupted. The majority of satellites that remain fully intact at present day were accreted recently without experiencing more than one pericentre ($n_{\rm peri} \lesssim 1$) and have large apocentres ($r_{\rm apo} \gtrsim 200\,{\rm kpc}$) and pericentres ($r_{\rm peri} \gtrsim 50\,{\rm kpc}$). The remaining satellites have experienced significant tidal disruption and, given full knowledge of the system, would be classified as stellar streams. We find stellar streams in Auriga across the range of pericentres and apocentres of the known Milky Way dwarf galaxy streams and, interestingly, overlapping significantly with the Milky Way intact satellite population. We find no significant change in satellite orbital distributions across resolution. However, we do see substantial halo-to-halo variance of ($r_{\rm peri}, r_{\rm apo}$) distributions across host galaxies, as well as a dependence of satellite orbits on host halo mass–systems disrupt at larger pericentres and apocentres in more massive hosts. Our results suggest that either cosmological simulations (including, but not limited to, Auriga) are disrupting satellites far too readily, or that the Milky Way's satellites are more disrupted than current imaging surveys have revealed. Future observing facilities and careful mock observations of these systems will be key to revealing the nature of this apparent discrepancy.

Key words: methods: numerical – Galaxy: halo – Galaxy: kinematics and dynamics – Galaxy: structure.

1 INTRODUCTION

In the standard Λ Cold Dark Matter (ΛCDM) paradigm, galaxies like the Milky Way (MW) experience a series of merger and accretion events (Searle & Zinn 1978). Many of these accreted systems are less massive dwarf galaxies, which first orbit the host galaxy before being disrupted by the tidal forces of the host's gravitational potential and ultimately phase-mix into a smoother stellar halo (Bullock & Johnston 2005). We therefore expect galaxies like our own to be surrounded by populations of *intact satellite galaxies,* systems currently undergoing tidal disruption such as extended *stellar streams,* and a smooth stellar halo consisting of the *phase-mixed* remnants of past accretion events.

Observations of the MW's halo have indeed revealed such structures. In particular, large, wide-area photometric surveys including the Sloan Digital Sky Survey (SDSS; York et al. 2000), the Dark Energy Survey (DES; DES Collaboration 2016), and other DECam surveys (Drlica-Wagner et al. 2021), have enabled the discovery of > 50 surviving satellite galaxies around the MW (e.g. Drlica-Wagner et al. 2020). These surveys, as well as the all-sky astrometric survey by the *Gaia* satellite, have also revealed large numbers of tidally disrupting stellar streams (e.g. Belokurov et al. 2006; Grillmair 2006; Koposov et al. 2014; Bernard et al. 2016; Malhan & Ibata 2018; Shipp et al. 2018), with the total number of stream candidates now exceeding 100 (Mateu 2023; Bonaca & Price-Whelan 2025). The majority of these stellar streams are confirmed or believed to have globular cluster progenitors, with only eight distinct streams confirmed to originate from dwarf galaxies (Li et al. 2022). The unprecedented proper motion measurements of MW stars by *Gaia*,

as well as radial velocity measurements from spectroscopic surveys, has also revealed an abundance of more phase-mixed structures in the MW's stellar halo, most notably the *Gaia*-Sausage-Enceledus (GSE) merger (Belokurov et al. 2018; Helmi et al. 2018; Naidu et al. 2020). Furthermore, these observations of the kinematics of stars in the MW's halo have enabled unprecedented dynamical characterization and modelling of these accreted systems (e.g. Kallivayalil et al. 2018; Erkal et al. 2019; Patel et al. 2020; Shipp et al. 2021; Pace, Erkal & Li ; Koposov et al. 2023).

Additionally, these rich data sets have exposed the complexity of these systems, and the difficultly in separating out truly intact from disrupting satellites. For example, many intact satellites have been found to have stars beyond their tidal radii (e.g. Carlin & Sand 2018; Chiti et al. 2021; Filion & Wyse 2021; Ji et al. 2021; Li et al. 2021; Qi et al. 2022; Sestito et al. 2023; Jensen et al. 2024; Ou et al. 2024b), although in many cases the cause of these extratidal stars remains uncertain, with explanations including tidal disruption due to the main host (Fattahi et al. 2018; Ou et al. 2024b), accretion from smaller systems (Tarumi, Yoshida & Frebel 2021; Deason et al. 2022), internal feedback mechanisms (Revaz & Jablonka 2018), and alternative models of dark matter (Pozo et al. 2024). Comparisons between the observed MW accreted satellite population and cosmological simulations of MW-like galaxies may help us to identify the origin of these extended stellar distributions, and to broaden our understanding of the full population of satellites around our own Galaxy.

Studies of intact satellite galaxy populations across simulations have long produced important results on the physics of small-scale galaxy formation (e.g. Brooks & Zolotov 2014; Sawala et al. 2016; Wetzel et al. 2016; Garrison-Kimmel et al. 2019; Grand et al. 2021; Munshi et al. 2021), constraints on the properties of dark matter (e.g. Bullock & Boylan-Kolchin 2017; Nadler et al. 2021; Sales, Wetzel & Fattahi 2022), and insight into the formation history of our own Galaxy (e.g. Rocha, Peter & Bullock 2012; Gómez et al. 2013; Fattahi et al. 2019; Bose et al. 2020; Fattahi et al. 2020; Samuel et al. 2020; Vera-Casanova et al. 2022). Only recently have hydrodynamic cosmological simulations reached resolutions that enable similar population-level studies of disrupting satellites around MW-mass hosts. Panithanpaisal et al. (2021) and Shipp et al. (2023) studied populations of stellar streams in the Feedback in Realistic Environments (FIRE-2) cosmological simulations. They classified accreted systems around 13 MW-mass host galaxies as intact dwarf galaxies, coherent stellar streams, or phase-mixed systems and produced synthetic observations of the simulated data in order to make comparisons to the observed MW stellar streams. They found that the number and stellar mass function of detectable streams around the FIRE-2 galaxies are consistent with those observed around the MW. However, they identified a discrepancy in the orbits of these systems, finding that even the *detectable* stellar streams in FIRE-2 disrupted at larger pericentres and apocentres than those in the MW, and that nearly all of the FIRE-2 satellites on orbits consistent with the MW streams have been fully phase-mixed. In addition, they found that many systems that have extended tidal tails would only be detected as intact satellites given the surface brightness limits of current surveys like DES. These conclusions raise the question of whether satellite galaxies are disrupting at artificially high rates in simulations, or whether the MW satellite galaxy population may in fact be more disrupted than previously observed. Distinguishing between these possibilities requires studies of disrupting satellites across simulations with a range of simulation codes, sub-grid physics models, host galaxy properties, and simulation resolutions.

In this work, we present a dynamical study of disrupting satellites in the Auriga cosmological simulations. We derive the orbital properties of the full population of accreted satellite galaxies, at all stages of tidal disruption, across 28 simulated MW-mass hosts at three different resolutions. In Section 2 we introduce the Auriga simulations used in this work, as well as their populations of intact satellite galaxies, stellar streams, and phase-mixed systems. In Section 3 we present the orbital properties of these systems, and discuss how orbits vary with satellite and host properties as well as simulation resolution. In Section 4 we summarize our conclusions and discuss the implications of the results for populations of disrupting satellites across simulations and in the MW. This paper accompanies Riley et al. 2024, hereafter Paper I, which presents the catalogue of accretion events in Auriga.

2 DISRUPTING SATELLITES IN AURIGA

2.1 Auriga simulations

The Auriga project (Grand et al. 2017, 2024) consists of cosmological, magnetohydrodynamic zoom-in simulations of 30 MW-mass galaxies (Au-1 to Au-30). These galaxies have halo masses (M_{200c}[1]) within the range $1 - 2 \times 10^{12} \, M_\odot$ and have a range of accretion histories and other halo and galaxy properties. These simulations were carried out using the moving-mesh code AREPO (Springel 2010; Pakmor et al. 2016) and include a comprehensive galaxy formation model that incorporates primordial and metal-line cooling (Vogelsberger et al. 2013), a spatially uniform redshift-dependent UV background for reionization (Faucher-Giguère et al. 2009), star formation and feedback mechanisms (Springel & Hernquist 2003; Vogelsberger et al. 2013), magnetic fields (Pakmor et al. 2017), and the modelling of black holes, including seeding, accretion, and feedback (Springel, Di Matteo & Hernquist 2005; Marinacci, Pakmor & Springel 2014; Grand et al. 2017).

The Auriga haloes were selected from the EAGLE dark-matter-only simulation box with a co-moving side length of 100 Mpc (Schaye et al. 2015), chosen not only for their specific mass range but also for their relative isolation.[2] The simulations use the cosmological parameters from Planck Collaboration XVI (2014), with $\Omega_M = 0.307$, $\Omega_\Lambda = 0.693$, $h = 0.6777$, $\sigma_8 = 0.8288$, and $n_s = 0.9611$. Initial conditions were generated using PANPHASIA (Jenkins 2013).

In this work we use three different resolution levels of these simulations. We consider 28 haloes that have been simulated at level 4[3], with dark matter particle mass, baryonic particle mass, and minimum particle softening length equal to $m_{DM} = 3 \times 10^5 \, M_\odot$, $m_b = 5 \times 10^4 \, M_\odot$, $h_b = 375$ pc. Six haloes (Au-6, Au-16, Au-21, Au-23, Au-24, Au-27) have been resimulated at level 3 ($m_{DM} = 4 \times 10^4 \, M_\odot$, $m_b = 6 \times 10^3 \, M_\odot$, $h_b = 188$ pc), and one halo (Au-6) has been resimulated at level 2 ($m_{DM} = 4.6 \times 10^3 \, M_\odot$, $m_b = 850 \, M_\odot$, $h_b = 94$ pc; Grand et al. 2021). We consider level 3 to be our fiducial resolution level. This mass resolution is roughly equivalent to that of the FIRE-2 *Latte* simulations (Wetzel et al. 2016) used in

---

[1]Defined to be the mass enclosed in a sphere in which the mean matter density is 200 times the critical density $\rho_{crit} = 3H^2(z)/8\pi G$. Virial quantities are defined at this radius and identified with a '200c' subscript.

[2]While the selection of isolated galaxies aids in reducing computational expense, it does mean that none of the selected galaxies have a M31-mass system nearby, which is an important caveat when comparing Auriga satellites to the MW satellite population.

[3]We exclude Au-1 and Au-11 because they are undergoing massive accretion events at $z = 0$.

previous studies of disrupting satellites by Shipp et al. (2023), and strikes a balance between halo sample size and simulation resolution. We present a study of satellite orbits across all three resolution levels in Section 3.3, and consider the larger sample of level 4 simulations to study the effect of host galaxy properties on satellite orbits in Section 3.4.

Halo catalogues in the Auriga simulations are generated using the on-the-fly SUBFIND halo finder (Springel et al. 2001). This process begins with a Friends-of-Friends (FOF) algorithm that groups dark matter particles into potential haloes based on a standard linking length criterion (Davis et al. 1985). Once these haloes are identified, the SUBFIND algorithm further refines the results by separating each halo into gravitationally self-bound subhaloes, ensuring that the catalogue accurately reflects the complex structure of these systems. The FOF algorithm initially groups only dark matter particles, while other particle types, such as gas, stars, and black holes, are assigned to the nearest dark matter group. SUBFIND is then applied across all particle types within each FOF group simultaneously. The merger trees are then constructed in post-processing with the LHaloTree algorithm (Springel 2005), enabling precise tracking of individual haloes, subhaloes, and their interactions over cosmic time. This method effectively traces the assembly and growth of galaxies within the Auriga framework.

The Auriga simulations accurately capture observed characteristics of spiral galaxies, including stellar masses, sizes, rotation curves (Grand et al. 2017), magnetic fields (Pakmor et al. 2017), and the distribution of neutral hydrogen (H I; Marinacci et al. 2017). Moreover, the Auriga simulations have played a crucial role in investigating the structure and dynamics of satellite galaxy systems (Simpson et al. 2018) and stellar haloes (Monachesi et al. 2016, 2019; Vera-Casanova et al. 2022), as well as offering insights into the MW's assembly history (Deason et al. 2017; Fattahi et al. 2019). The Auriga simulations have also contributed to understanding the orbits of the MW's satellites (Riley et al. 2019) and have been used to estimate the mass of the MW, producing results that align well with a range of observational constraints (Callingham et al. 2019; Deason et al. 2019). We build our analysis on the foundation of these works, with a particular focus on the results exploring satellite dynamics and their interactions with the host galaxy.

2.2 Catalogue of disrupting satellites

The Auriga catalogue of disrupting satellites is presented in detail in Paper I. In short, we first identify all of the accretion events across the history of each of the 28 simulated host galaxies. We then identify all of the simulation star particles associated with each accretion event (regardless of whether they are currently bound to the accreted system) and determine their positions and velocities at $z = 0$. Due to resolution limits, we consider all accretions with > 100 associated star particles. This corresponds to $M_* \sim 5 \times 10^6$, 6×10^5, and $8.5 \times 10^4 \, \mathrm{M_\odot}$ at levels 4, 3, and 2, respectively. Among our sample, this stellar mass limit corresponds to haloes with $\gtrsim 10^4$ dark matter particles.

We then classify systems as *intact satellite*, *stellar stream*, or *phase-mixed*. We determine whether a satellite remains intact based on the fraction of associated stars that are bound to the satellite progenitor at $z = 0$. Intact satellites are defined as systems with $f_{\mathrm{bound}} > 0.97$. We differentiate between coherent streams and phase-mixed structures based on the median local velocity dispersion (σ_{50}) of the star particles associated with each system. Systems are classified as phase-mixed if $\sigma_{50} > 3.51 \log \left(\frac{M_*}{M_\odot} \right) + 1.08$, where

the coefficients are fit via a support vector machine model applied to a visually classified sample. This technique was first used to classify tidal debris as coherent stream or phase-mixed in the FIRE-2 simulations by Panithanpaisal et al. (2021), and the method as applied to Auriga is described in greater detail in Paper I.[4] An important point to note is that we have made no correction for the detectability of the Auriga systems; as in Shipp et al. (2023), many systems with tidal debris are likely too faint to detect, or would only be detected as intact progenitors given current imaging.

Typically we find that the majority of accretion events that we catalogue have been phase-mixed, followed by a significant fraction of systems (~ 30 per cent) that are currently undergoing tidal disruption and are classified as stellar streams, and a relatively small fraction of accretions ($\lesssim 10$ per cent) that survive to $z = 0$ as intact satellites. This can be seen in Fig. 1, which illustrates the complete accreted satellite population around one of the simulated Auriga haloes (Au-23), divided by morphological classification. *Notably, the majority of systems with surviving progenitors also have extended tidal tails and are classified as stellar streams.*

3 ORBITAL PROPERTIES OF DISRUPTING SATELLITES

3.1 Orbit fitting

To determine the orbital properties of each disrupting satellite, we trace the positions of each member star particle back through the output simulation snapshots. The frequency of snapshots varies across resolution level. Near $z = 0$ the snapshot spacing is $\sim 130 \, \mathrm{Myr}$ for level 4, $\sim 330 \, \mathrm{Myr}$ for level 3, and for level 2 the star particles are output at a higher frequency of $\sim 10 \, \mathrm{Myr}$. The level 2 snapshots are saved at a high enough frequency to reliably recover the pericentres and apocentres of the system. However, for both level 4 and level 3 we integrate the orbits between snapshots in order to ensure we are calculating the pericentre and apocentre to sufficient accuracy.

To do this, we use SUBORBITIN (Richings et al. 2020) and AGAMA (Vasiliev 2019) to model the potential of the host galaxy near each pericentre snapshot and to integrate the satellites orbits. Following the well-established method of simulation orbit reconstruction using basis function expansions (Sanders et al. 2020; Arora et al. 2022, 2024), we describe the host galaxy potential via a multipole expansion with $l_{\mathrm{max}} = 4$, using a combination of spherical harmonics and azimuthal harmonics for the halo and disc, respectively. We then compute a weighted average of the potential of the two snapshots nearest to the calculated pericentre or apocentre and integrate the orbit in this combined potential. One simulated galaxy (Au-18) was resimulated with an ultrahigh frequency snapshot cadence of $\sim 5 \, \mathrm{Myr}$. We test our orbit fitting method on this simulation and confirm that we can indeed accurately recover even small pericentres at the snapshot frequencies of the level 4, 3, and 2 simulations.

We define the pericentre (apocentre) as the most recent closest (farthest) approach to the centre of the host galaxy of the progenitor orbit. This is most analogous to what is measured for observed systems, and consistent with the values presented for the FIRE-2 simulations in Shipp et al. (2023). For intact satellites and stellar streams, we identify the $z = 0$ progenitor location by fitting a 3D Gaussian kernel density estimate (KDE) to the spatial coordinates of

---

[4]In this classification scheme, shells – disrupting systems that may be extended both parallel and perpendicular to their progenitor orbit – would primarily be classified as phase-mixed.

Figure 1. Complete population of accreted satellites, including intact satellites (left), streams (middle), and phase-mixed systems (right) around one of the Auriga haloes (Au-23, level 3), shown in the simulation's Cartesian coordinate system centred on the host galaxy. Only a small fraction of accreted systems remain intact and many of the surviving progenitors have extended tidal tails and are classified as stellar streams. The colours are assigned to each accreted satellite arbitrarily in order to differentiate the member stars between systems. An animation of the positions of these systems over time can be found at this url.
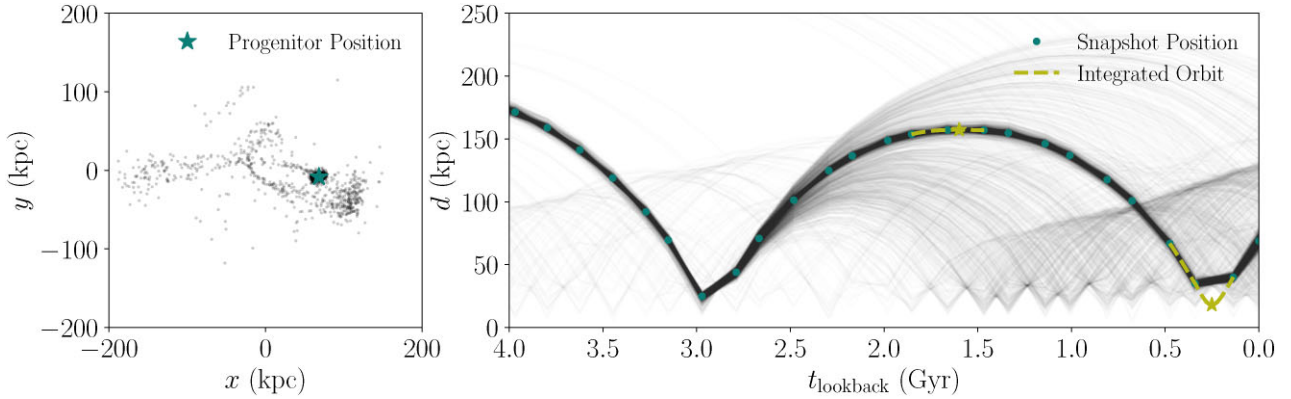

Figure 2. Example stream orbit demonstrating the process of calculating pericentres and apocentres of simulated satellites. The left panel shows the spatial distribution of the member stars of a simulated stellar stream, and the high-density progenitor region is marked by a blue star. On the right, the distance as a function of lookback time is shown for each member star (thin lines). The points indicate the median position of the selected progenitor stars from the simulation snapshots. The dashed curves show the integrated orbits around the pericentre and apocentre and the stars show the calculated pericentre and apocentre values.

the member stars. We select stars residing within the highest density region, take the median of their position and velocity coordinates (which we consider to represent the progenitor location) and integrate the progenitor orbit using the above method. By first calculating the progenitor position at each snapshot and then considering the bulk progenitor orbit rather than the orbit of each individual member star, in addition to interpolating between snapshots using the weighted averaging framework of Richings et al. (2020), we eliminate the need to consider the self-gravity of the progenitor during the integration. For phase-mixed systems as well as a small number of streams, which no longer have a high-density region corresponding to the progenitor location, we integrate the orbits of each individual member star, then take the median pericentre and apocentre values.

A small subset of systems have not had a pericentre and/or apocentre after accretion, where accretion is defined as the first time of crossing R_{200c} of the host galaxy. In that case we consider their current distance to be an upper limit on the pericentre and lower limit on the apocentre. These values are plotted as upper/lower limits in any figures where they are included.

Fig. 2 illustrates the orbit fitting procedure for one example stream. The left-hand panel shows the spatial coordinates of the stream member stars at $z = 0$, with the selected progenitor location highlighted with a blue star. The right-hand panel shows the distance of each member star from the centre of the host galaxy over time. The stars in the high-density progenitor region can be identified as the thick black line from which other orbits diverge over time. The snapshot progenitor positions are plotted as blue points and the integrated orbits around pericentre and apocentre are shown in yellow. The final pericentre and apocentre values are indicated with yellow stars. This example highlights the need to model orbits where snapshot cadences are sparse – using only the snapshot positions of the star particles would give a most recent pericentre of ∼40 kpc, while interpolating between snapshots yields ∼20 kpc.

3.2 Satellite orbits

Fig. 3 presents the pericentres and apocentres of intact satellites, stellar streams, and phase-mixed systems across the Auriga simulations. Systems from the fiducial level 3 simulations are shown as
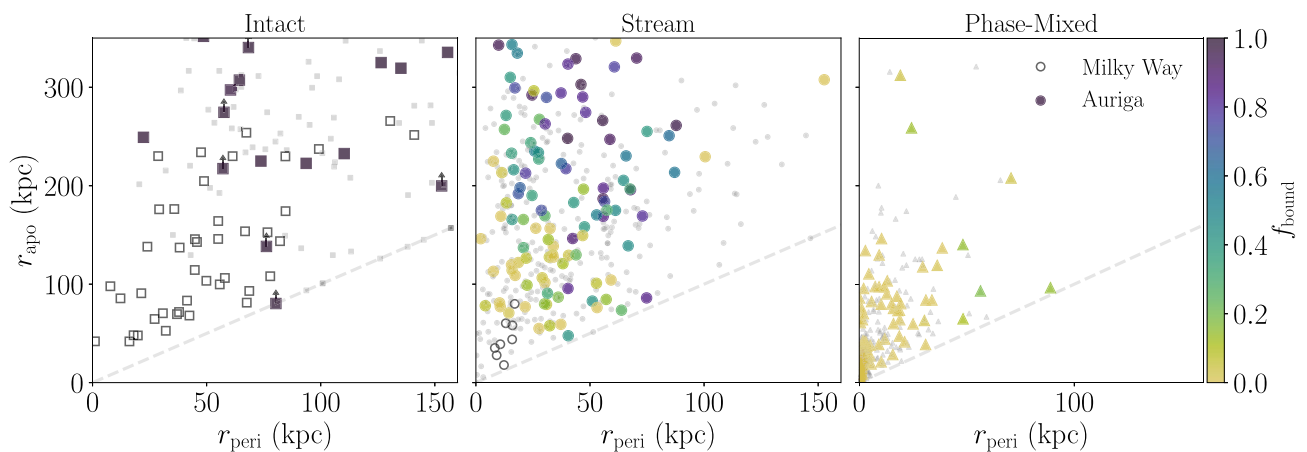
Figure 3. Pericentres and apocentres of intact satellites (left panel), stellar streams (middle panel), and phase-mixed systems (right panel) in the Auriga simulations. The fiducial level 3 simulations are coloured by the fraction of associated stars that remain bound to the progenitor at $z = 0$ (by definition, all intact systems have $f_{\rm bound} \sim 1$). Other resolutions (level 4 and level 2) are plotted in the background as light grey points to illustrate the variation across the full sample of 28 simulated host galaxies. The dashed grey line indicates circular orbits (equal pericentre and apocentre). The unfilled markers represent the MW satellites (squares) and streams (circles) for comparison, see Section 3.2 for data sources. Note that there is no completeness or detectability correction applied here, so some of the Auriga systems may not be detectable given current observations.

coloured points, where the colour corresponds to the fraction of stars that remain bound at $z = 0$. Level 2 and 4 systems are included as grey background points to demonstrate the broad range across the 28 unique host galaxies. The left panel shows the intact satellites (squares). The unfilled boxes indicate the MW satellite orbits from Pace et al. (2022). These orbits are calculated in a static three-component MW potential, plus an infalling LMC and the resulting reflex motion of the centroid of the MW. We assign satellites with confirmed tidal tails (Sagittarius and Tucana III) as streams, but include satellites such as Crater II and Antlia II which have proposed signs of tidal disruption (Torrealba et al. 2019; Ji et al. 2021; Pace et al. 2022; Vivas et al. 2022) as intact. It is highly likely that some of the simulated systems would not yet be detectable in our Galaxy given available data. We leave mock observations of the Auriga streams for future work. Note that several intact satellites are recently accreted and have not had a pericentre and/or apocentre after accretion and are therefore plotted with their current distance as an upper/lower limit, as discussed in Section 3.1.

The middle panel shows the systems classified as stellar streams (circles). The unfilled points represent the MW dwarf galaxy streams. The pericentre and apocentre values are taken from Li et al. (2022). As for the intact satellites, the stream orbits are calculated in a MW potential that includes the effect of an infalling constant-mass LMC and the reflex motion of the MW, but does not include any other time dependence of the potential. The right panel shows the phase-mixed systems (triangles). No MW systems are plotted in this case, because of the difficulty in measuring orbital parameters for observed phase-mixed structures. We note that the pericentres and apocentres for the phase-mixed systems in Auriga are generally less informative than for the streams and satellites due to the large spread in orbits among member stars and the impossibility of selecting only the progenitor orbit (Khoperskov et al. 2023; Mori et al. 2024). The axis limits of the figure are limited to highlight the range overlapping with the MW systems.

The full extent to the pericentre–apocentre distributions is shown in Fig. 4, where the level 3 points are coloured by lookback time to accretion and the level 4 and 2 systems are again plotted as background grey points. Importantly, we find that the Auriga simulations do include several cases of streams and even phase-mixed
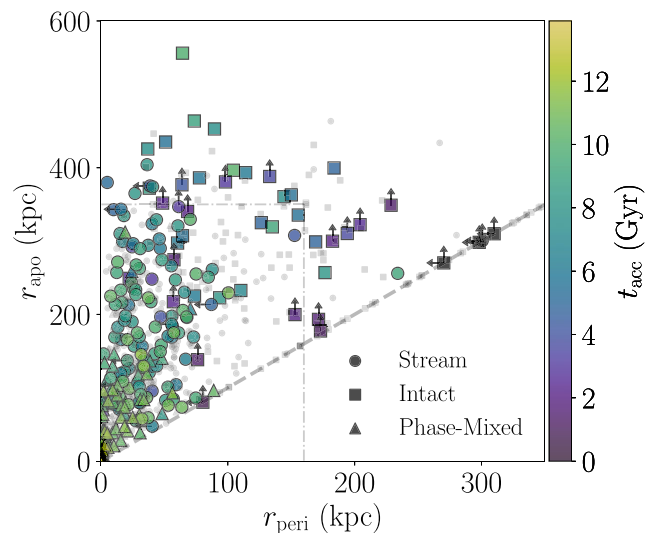

Figure 4. Full range of pericentres and apocentres of intact satellites (squares), stellar streams (circles), and phase-mixed systems (triangles) in Auriga. The fiducial level 3 simulation points are coloured by the lookback time to accretion of each system. The level 4 and level 2 resolution points are included as light grey points in the background. The thick grey-dashed line indicates circular orbits, and the light dashed grey box indicates the axis limits shown in Fig. 3. At large pericentres and apocentres there are several intact satellites on first infall, that have not had a pericentre or apocentre since accretion and are therefore shown with their current distance as an upper/lower limit.

systems forming around satellites, which can lead to deceptively large pericentres and apocentres for disrupted systems. This affects the overall pericentre and apocentre distributions, but largely only contributes significant outliers that can be seen in Fig. 4 and does not bias the distribution shown in Fig. 3. The effect of satellites-of-satellites will be discussed in greater detail in Section 3.4.1.

Fig. 5 shows the accretion time and eccentricity of systems classified as intact (squares), streams (circles), and phase-mixed (triangles) coloured by their stellar bound fraction. This figure includes only
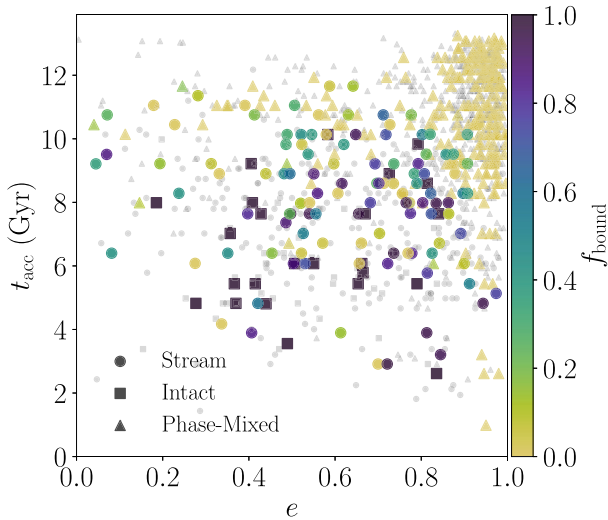
Figure 5. Lookback time to accretion versus orbital eccentricity of disrupting satellites in Auriga. As in the previous figures, the fiducial level 3 simulation points are coloured by the stellar bound fraction of each system, while the other resolution points are included in the background. Phase-mixed systems (triangles) nearly all follow very eccentric orbits and/or were accreted > 10 Gyr ago. Streams and intact satellites follow a broader distribution, however intact satellites generally have been accreted more recently, and if not tend to be on more radial orbits with very large apocentres.

systems that have had a pericentre and apocentre since accretion and therefore have a well-defined orbital eccentricity. All of these figures are discussed in greater detail in the following subsections.

3.2.1 Intact satellites

Intact satellites in Auriga tend to be orbiting at large apocentres, fairly large pericentres, and to have completed a small number of orbits since accretion. In particular, all intact satellites (that have a calculated apocentre) have $r_{\mathrm{apo}} > 200\,$kpc, in contrast with the large population of MW satellites at much smaller apocentres. In addition, with some exceptions, the intact Auriga satellites have $r_{\mathrm{peri}} > 50\,$kpc, again in apparent disagreement with observed MW satellites. By definition, the intact satellites have large values of $f_{\mathrm{bound}} > 0.97$. In Figs 4 and 5, it can be seen that the majority of intact satellites, particularly if they have smaller pericentres or apocentres, were accreted recently ($t_{\mathrm{acc}} < 6\,$Gyr). Earlier-accreted intact systems tend to be on more radial orbits ($e > 0.5$) and therefore have large apocentres and have spent less time in the inner galaxy (the few with $e < 0.5$ have large pericentres). In fact, we find that most intact satellites have not experienced more than one pericentre (across the level 3 simulations, ~ 25 per cent have had zero pericentres, ~ 60 per cent have had one, and ~ 15 per cent have had two).

There is an apparent discrepancy between the orbits of the Auriga intact satellites and those of the observed MW satellites, which could be due to a range of observational, theoretical, or numerical effects. On the theoretical side, there are both uncertainties when computing the MW satellite orbits (D'Souza & Bell 2022; Santistevan et al. 2024) and potential overdisruption in the simulations (due to numerics or galaxy formation or dark matter models). If the simulations are correct, then it could be that the 'intact' MW satellite population is in fact more disrupted than has so far been observed and would be classified as streams under our framework (if they have lost more than 3 per cent of their stellar mass).

Shipp et al. (2023) showed that the uncertainty due to the fact that the MW satellite orbits are integrated in a largely time-independent potential is negligible relative to the scale of the differences, suggesting that uncertainty on measured orbital parameters cannot account for the full discrepancy. Properties of the simulations and the possibility of overdisruption will be discussed in greater detail in Section 4. A key remaining uncertainty lies in the detectability of the Auriga satellites. Shipp et al. (2023) found that in the FIRE-2 *Latte* simulations, many disrupting satellites would be misclassified as intact in DES-depth data, given the low surface brightness of their tidal tails relative to the high-density progenitor. This is likely true for many of the Auriga satellites as well and will be addressed in future work. The apparent discrepancy between the orbits of intact satellites in Auriga and the MW will be discussed in greater detail in Section 4.

3.2.2 Stellar streams

The Auriga stellar streams span the broadest range of pericentre–apocentre space, extending from very small values (r_{peri}, $r_{\mathrm{apo}} < 10\,$kpc) to, in rare cases, $r_{\mathrm{peri}} > 100\,$kpc, $r_{\mathrm{apo}} > 300\,$kpc. There is significant variation in f_{bound} between values of 0 and 0.97 and a strong correlation with orbital radius, with streams with $r_{\mathrm{peri}} \lesssim 50\,$kpc and $r_{\mathrm{apo}} \lesssim 150\,$kpc having lost nearly all of their stars. In Auriga, only ~ 30 per cent of stellar streams have $f_{\mathrm{bound}} < 5$ per cent, whereas the majority of the known MW dwarf galaxy streams (> 80 per cent, with only the exception of Sagittarius and Tucana III) do not have known associated progenitors. Given the small pericentres and apocentres of the MW streams, this picture is not inconsistent with the low f_{bound} of Auriga streams on similar orbits.

However, there is a notable difference between the apparent orbital distributions of the simulated and observed stellar streams, with streams forming in the Auriga simulations at much larger pericentres and apocentres than we have yet to observe in the MW. Furthermore, the majority of Auriga systems on orbits consistent with the surviving MW satellite population are classified as stellar streams and have lost a significant fraction of their stellar mass ($f_{\mathrm{bound}} \lesssim 0.8$). This apparent discrepancy hints at gaps in our understanding of satellite galaxy formation and evolution in MW-like systems. Possible explanations are discussed in the following sections, including numerical effects (Section 3.3) and host galaxy properties (Section 3.4). In addition, a key point to keep in mind is that we have made no completeness correction to the MW distribution, nor have we evaluated the detectability of the simulated stellar streams. It is possible that, after conducting mock observations, many of the Auriga streams would be misclassified as intact satellites that have experienced no disruption, given current observational capabilities. In fact, recent observations have revealed more and more evidence of extra-tidal features around MW satellites (e.g. Jensen et al. 2024), suggesting that they are likely to be more disrupted than we had previously observed. This possibility is discussed in greater detail in Section 4.

In the FIRE-2 simulations, Shipp et al. (2023) observed that accreted satellites on orbits consistent with the MW dwarf galaxy streams are almost entirely phase-mixed. This is also true for the limited sample of six resolution level 3 simulations, but is not true across all resolution levels. In Fig. 3, it can be seen that there are several systems among the full sample of 28 haloes (grey points) with smaller pericentre and apocentre values that are consistent with the MW observed streams. In particular, 4 streams from Au-7 and 3 streams from Au-(4, 5, 15, 21, 22) have $r_{\mathrm{peri}} < 25\,$kpc and
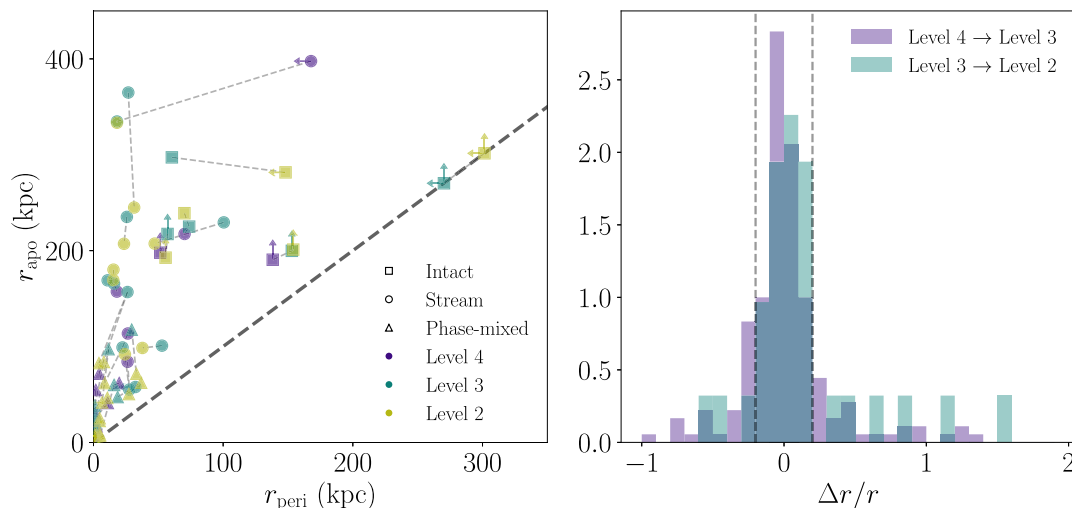
Figure 6. Pericentres and apocentres of satellites of Au-6 across three resolution levels (left). Squares represent intact satellites, circles represent stellar streams, and triangles represent phase-mixed systems. The points are coloured by corresponding resolution, from highest resolution level 2 (yellow), to the fiducial resolution level 3 (blue), to the lowest resolution level 4 (purple). Systems that are matches across resolutions are connected by dashed lines. The histograms (right) show the fractional change in pericentres and apocentres of all intact satellites and stellar streams matched between resolution levels. The majority of systems lie within the dashed lines indicating ±20 per cent change. The more significant changes generally correspond to changes in accretion time and thereby in number of pericentres since accretion.

$r_{apo} < 100$ kpc (note that the minimum stellar mass we consider in level 4 is 3.7×10^6 M$_\odot$) and 20 haloes have at least 1 stream within those limits. We find significant halo-to-halo variance between the simulated MW-mass galaxies, suggesting that larges sample of both simulated and observed stream populations is necessary to fully assess the consistency of the MW with predicted stream populations in ΛCDM. This finding is consistent with the results of studies of semi-analytic models of large numbers of stream populations around MW-mass hosts (Dropulic et al. 2024). The effect of halo-to-halo variance, as well as possible trends with host properties, will be discussed in greater detail in Section 3.4.

In Fig. 4, there are a small number of stellar streams with $r_{peri} > 150$ kpc. These are all classified as satellites-of-satellites and have been disrupted by another galaxy than the main host. This effect will be discussed in greater detail in Section 3.4.1.

The Auriga stellar streams also span a large range of accretion times and orbital eccentricities, as seen in Figs 4 and 5. Among the stellar streams, we do not find a strong correlation between accretion time or eccentricity and f_{bound}.

Finally, we find no strong preference for either prograde or retrograde orbits among the Auriga stellar stream population as whole. We do however find that some individual simulations have a larger number on either prograde or retrograde orbits, which may be due to the accretion history of the particular host galaxy. This suggests that the fact that the MW streams lie almost exclusively on prograde orbits (Li et al. 2021) may be due to the particular accretion history of the MW rather than a generic outcome of tidal disruption by a MW-like host galaxy.

3.2.3 Phase-mixed systems

Phase-mixed systems in Auriga tend to have early accretion times ($t_{acc} > 8$ Gyr) or highly eccentric orbits ($e > 0.8$), and most have both, as seen in Fig. 5. The right-hand panel of Fig. 3 illustrates the pericentres and apocentres of the phase-mixed systems, which tend to have very small pericentre and apocentre values (< 10 kpc). A

relatively small number of systems have larger orbital radii. However, as mentioned above, the orbits of phase-mixed systems are most difficult to define, even in simulations. For all accreted systems we calculate the most recent pericentre and apocentre. Many of the phase-mixed systems have experienced a large number of pericentres and the orbits of their member stars often diverge significantly. The larger values are in many cases therefore not representative of the closest approach distance of the system across its entire history, but of the current median orbit of the member stars. Some of the systems with the largest pericentres have also been identified as satellites-of-satellites and will be discussed in Section 3.4.1.

3.3 Effect of simulation resolution

Satellite galaxy populations in simulations can be impacted by the effects of numerical resolution (Grand et al. 2021). In order to quantify these effects on the disrupting satellite populations in Auriga, we compare satellites simulated across the three resolutions (level 4, 3, and 2 as described in Section 2).

In particular, we compare the six host galaxies that have been simulated at both level 4 and level 3 resolution, including the single galaxy (Au-6) that has been resimulated at the highest resolution, level 2. For each resimulated galaxy, we match accretion events across resolution by comparing the initial positions of dark matter member particles. This procedure is described in detail in Paper I.

Paper I also discusses the impact of simulation resolution on disrupting satellite morphology. In short, we find that the morphological classifications are largely converged across resolution. Changes in classification are generally due to minor changes in stellar bound fraction (f_{bound}), local velocity dispersion (σ_{50}), or accretion time.

Here, we examine the orbits of disrupting satellites across resolution. Fig. 6 illustrates the changes in calculated pericentre and apocentre values. The left panel shows systems in Au-6 at all three resolutions, with lines connecting systems that have been matched across resolution. The right panel shows a histogram of the fractional shift in pericentres and apocentres (combined across all resimulated galaxies) from level 4 to 3 and from level 3 to 2. We define $\Delta r/r$
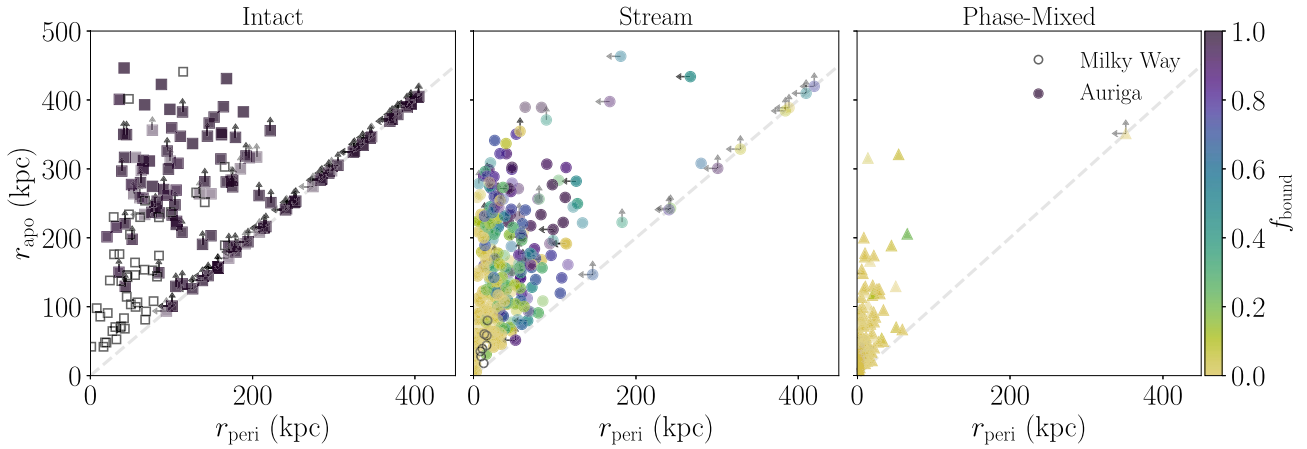
Figure 7. Pericentres and apocentres of intact satellites (left), stellar streams (middle), and phase-mixed systems (right) across the 28 level 4 host galaxies. All points are coloured by the stellar mass bound fraction $f_{\rm bound}$. Systems that are classified as satellites-of-satellites are plotted with a higher transparency. As in previous versions of this figure, systems that have not had a pericentre and/or apocentre since accretion are plotted with their current distance as a upper/lower limit on their pericentre/apocentre.

as $(r_{\rm low\ res} - r_{\rm high\ res})/r_{\rm high\ res}$. The vertical dashed lines indicate a ± 20 per cent fractional change. The majority of pericentres and apocentres have a shift of less than 20 per cent. For level 4 to 3, the median shift is -0.5 per cent and 124 of 188 of satellites have shifts smaller than 20 per cent. For level 3 to 2, the median shift is $+4$ per cent and 22 of 32 satellites have shifts less than 20 per cent. We note that the histograms are normalized, and the number of systems in the level 2 histogram is much smaller (32 versus 188), given that only Au-6 has been resimulated at the highest resolution. The median level 3 to 2 shift is positive (4 per cent), possibly suggesting that orbits tend to shift to smaller radii with increasing resolution. However, the sample size is small, and the stellar masses of the Auriga galaxies also tend to increase with increasing resolution (Grand et al. 2017, 2021), and it is expected that the satellite orbits would move inward as the central mass of the host galaxy increases. The outliers with $|\Delta r/r| > 0.5$ are systems that were accreted at slightly different times in the resimulation and therefore have had, for example, one fewer pericentre at one resolution than the other. These slight changes in orbital history are expected between realizations of varying random seed, regardless of change in resolution.

In summary, we find that the orbits of disrupting satellites in Auriga are well-converged across the three resolution levels presented here. Differences in the orbital distributions between the samples at different resolutions are largely due to halo-to-halo scatter and the effects of resimulating galaxies, and not varying systematically due to numerical resolution.

3.4 Effect of host galaxy properties

The orbits of disrupting satellites are sensitive to the properties of their host galaxies (Garrison-Kimmel et al. 2017; Riley et al. 2019; Dropulic et al. 2024). Understanding the effect of host properties, including the influence of massive satellites and the dependence on host halo and disc properties is essential for interpreting the MW's own satellite populations in the context of ΛCDM.

Here, we consider the 28 haloes simulated at level 4 and study the orbits of their satellite populations as a function of host galaxy and halo properties. As described in Section 2, these haloes were selected based on their mass ($1 - 2 \times 10^{12}\,{\rm M_\odot}$), and to be isolated at $z = 0$ (i.e. none of these galaxies have an Andromeda analogue).

The selected galaxies otherwise have a range of galaxy properties and accretion histories, which are discussed in more detail elsewhere (Grand et al. 2017; Monachesi et al. 2019; Fattahi et al. 2020; Vera-Casanova et al. 2022).

Fig. 7 shows the full distribution of pericentres and apocentres of satellites around the 28 level 4 host galaxies, including intact satellites (left panel), stellar streams (middle panel), and phase-mixed systems (right panel). Note that this figure shows the full range of values, unlike in Fig. 3, which is zoomed in to highlight the region overlapping with MW systems. Across these 28 simulations, there is a large spread in orbital parameters. However, we see that the intact satellites that have had an apocentre since accretion all have $r_{\rm apo} \gtrsim 200$ kpc. This emphasizes the apparent discrepancy with the MW satellite orbits (unfilled squares), many of which have smaller apocentre values. It is unlikely that this discrepancy is entirely due to properties of the MW itself or to halo-to-halo scatter, and supports the conclusion that either the MW satellites are more disrupted than has been so far observed or that a short-coming in our simulations (either numerical or theoretical) is leading to substantial overdisruption of satellite galaxies. Either conclusion would have important implications for studies of satellite galaxies in the context of ΛCDM.

A large number of systems across the 28 simulations have not had a pericentre or apocentre since accretion. The majority of these systems are classified as intact satellites, however, there are a significant number of stellar streams and a single phase-mixed system that are newly accreted, currently located at distances of $d > 200$ kpc, and yet have been tidally disrupted. These systems have been identified as satellites-of-satellites, are indicated by transparent markers, and are discussed in greater detail below.

3.4.1 Massive satellites

Massive satellites recently accreted on to the the host galaxy can significantly influence the population of surviving and disrupted satellite galaxies. The hierarchical theory of structure formation predicts that galaxies that are accreted on to hosts like the MW should in turn have accreted their own population of lower mass satellites (Li & Helmi 2008; Wetzel, Deason & Garrison-Kimmel 2015; Santos-Santos et al. 2021). In fact, the LMC, the most massive
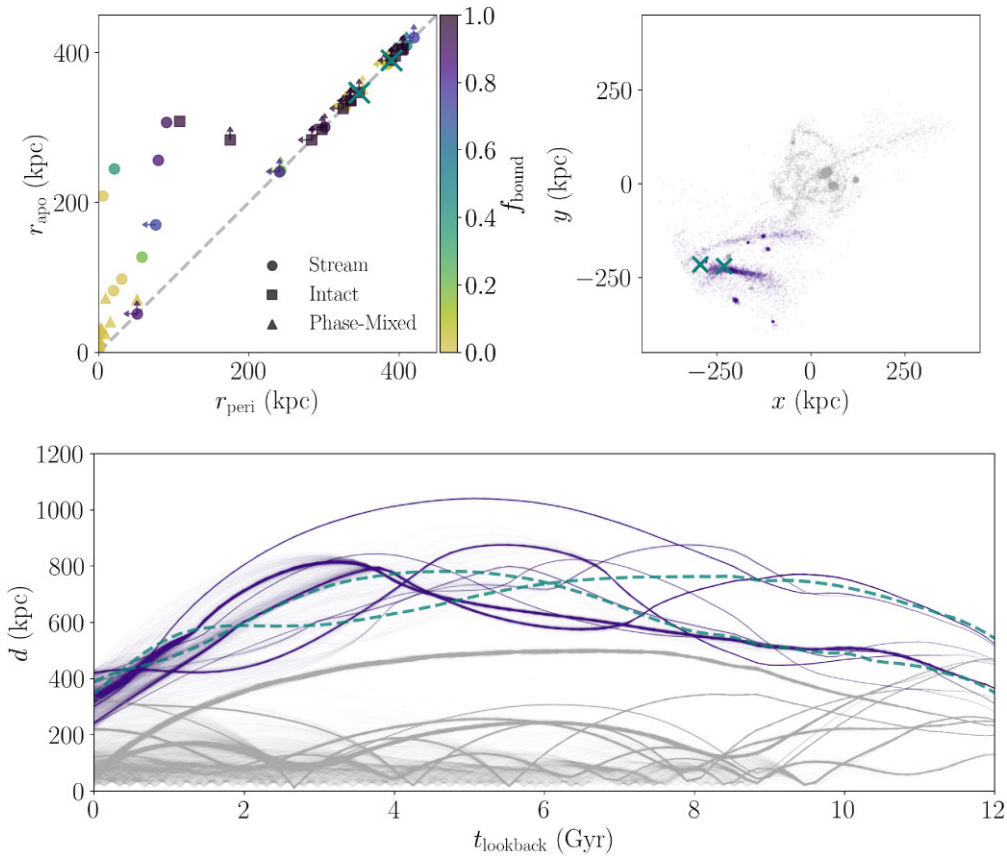
Figure 8. Orbits and positions of disrupting satellites around Au-18, a MW-mass galaxy with a recently accreted, ongoing merger with two massive satellites. The upper-left panel shows the pericentres and apocentres of intact satellites, stellar streams, and phase-mixed systems around Au-18. As in previous versions of this figure, systems that have not yet had a pericentre and/or apocentre after accretion on to the main host are shown with their current distances as upper/lower limits on pericentre/apocentre. The two massive merging satellites are marked as Xs. The upper right panel shows the $z = 0$ spatial distribution of systems classified as stellar streams around Au-18. The systems considered to be satellites of the massive objects are plotted in purple (darker), while all other streams are shown in grey (lighter). The two Xs indicate the centroids of the massive satellites. The lower panel shows the orbits over time of stellar streams around Au-18. Once again the satellites of the two massive satellites are shown in purple (darker) while all other streams are shown in grey (lighter). The orbits of the two massive systems are shown as dashed lines.

satellite of the MW, is thought to have brought in its own satellites (Kallivayalil et al. 2018; Nadler et al. 2020; Patel et al. 2020; Vasiliev 2024), and is known to have influenced the orbits, and possibly the disruption rates, of the MW stellar streams (e.g. Gómez et al. 2015; Erkal et al. 2018, 2019; Koposov et al. 2019; Shipp et al. 2021; Vasiliev, Belokurov & Erkal 2021; Koposov et al. 2023; Lilleengen et al. 2023; Brooks et al. 2024).

In this work, we classify systems as satellites-of-satellites if they are not the most massive halo in their FOF group (excluding the main host) for three consecutive snapshots (see Paper I for further detail). The satellites are identified in Fig. 7 as the points with a higher transparency. In particular, it is clear that nearly all of the streams that have not had a pericentre and/or apocentre since accretion are classified as satellites-of-satellites and have in fact been disrupted by pre-processing in another environment, not by the tidal field of the main MW-mass host galaxy. The majority of these systems come from a single simulated galaxy, Au-18, which has recently accreted a massive pair of satellites ($M_* = 2.7, 2.3 \times 10^{10} \, \text{M}_\odot$).

These satellites and their associated streams are shown in Fig. 8. The top left panel shows the pericentres and apocentres of all the satellites associated with Au-18. There are a large number that are on first infall and have not had a pericentre or apocentre since accretion and are therefore plotted at their current distance along

the circular orbit dashed line. The two blue X's indicate the two massive satellites, which are also on first infall into the host galaxy. The spatial distribution of the Au-18 stellar streams is shown in the upper right panel. The blue X's again indicate the location of the two massive satellites. The streams associated with these infalling systems are plotted in purple, while the rest of the Au-18 streams are shown in grey. The lower panel shows the distance over time of all the Au-18 stellar streams, as well as the blue lines indicating the orbits of the two massive satellites. It is clear that several streams are orbiting the massive satellites as the system falls into the main host potential. This explains their high disruption rates despite the lack of close passage to the main host. These streams have instead been disrupted by the massive satellites. The example highlights the importance of considering the effect of massive satellite systems and, more generally, the pre-processing of satellites before infall on to the main host. These effects can influence the overall distribution of pericentres and apocentres and lead to higher disruption rates at large distances from the host galaxy (He, Han & Li).

In addition, massive satellites can have more indirect effects on disrupting satellite populations. Satellites as massive as the LMC are known to cause significant, time-varying distortions to the MW potential (Gómez et al. 2016; Garavito-Camargo et al. 2021) which may have larger scale effects on the stream population as a whole.
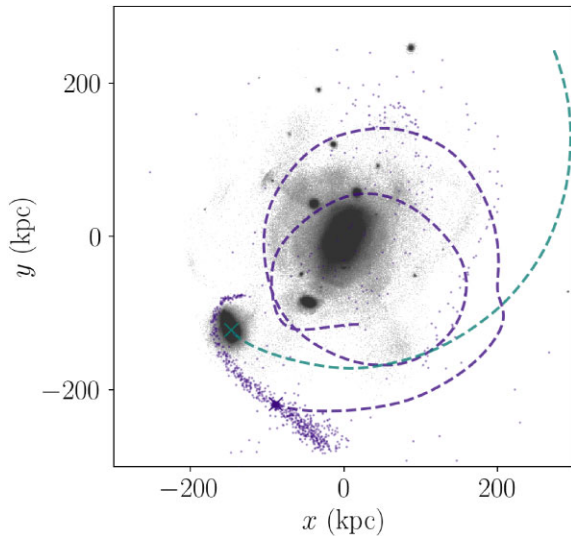
Figure 9. Example of a stellar stream perturbed by a massive satellite. The stream, plotted in purple (darker points), has been orbiting the host at a large distance ($r > 100\,\mathrm{kpc}$) for more than 9 Gyr (past orbit shown as the darker dashed purple line). However, despite its large distance, it is heavily disrupted ($f_{\mathrm{bound}} = 0.36$) due to perturbation by a massive satellite (past orbit shown as lighter turquoise dashed line). The X's indicate the positions at present day of the stream progenitor (darker purple) and the perturbing massive satellite (lighter turquoise). The background histogram shows the stars belonging to all of the accreted systems.

For example, Fig. 9 illustrates a stream that orbited the main host galaxy at a large distance ($r > 100\,\mathrm{kpc}$) for more than 9 Gyr with little consequence, and recently lost a substantial fraction of its stellar mass ($f_{\mathrm{bound}} = 0.36$) due to a close encounter with a massive satellite. These effects would benefit from further study of cosmological simulations with MW-like merger histories, including a massive LMC-like satellite.

3.4.2 Halo and disc properties

The properties of the host galaxy itself can also have a significant effect on disrupting satellite populations. In particular, the host mass is correlated with the number, mass function, and radial distribution of infalling satellites, and the disc contributes significantly to satellite disruption (Errani et al. 2017; Garrison-Kimmel et al. 2017; Nadler et al. 2018; Kelley et al. 2019; Wang et al. 2025). These effects propagate to the orbital distributions of satellites at all stages of tidal disruption.

In Fig. 10, we examine how the distributions of pericentres and apocentres of intact satellites and stellar streams depend on properties of the host halo and central disc. Once again, we consider the 28 level 4 simulations. Here we show the distributions binned by host halo mass (M_{200c}, top row), host galaxy disc size ($R_{50}^{\mathrm{in\ situ}}$, defined as the spherical radius that encloses 50 per cent of in situ stellar mass, middle row), and in situ stellar mass ($M_*^{\mathrm{in\ situ}}$, a proxy for disc mass, bottom row). These values for each simulation are compiled in table 1 of Paper I.

We find suggestions of dependence on the stream and intact satellite pericentre and apocentre distributions on each of these parameters. First, satellites at all stages of disruption seem to shift to larger orbits with increasing M_{200c}, which is expected as the size of the host galaxy potential grows. Although expected, this is an important point, given the significant uncertainty on the halo mass of

the MW (Callingham et al. 2019; Wang et al. 2020). Understanding discrepancies between predicted and observed orbits of disrupting satellites requires accounting for these uncertainties on the properties of the MW itself.

Secondly, satellites at smaller orbital radii seem to be less disrupted (larger f_{bound}) with increasing $R_{50}^{\mathrm{in\ situ}}$. Among this sample of galaxies, the disc size is not highly correlated with either disc mass or halo mass. This means that increasing $R_{50}^{\mathrm{in\ situ}}$ tends to decrease the density of the disc, which may allow satellites to retain more of their member stars while orbiting deeper in the galactic potential. Finally, $M_*^{\mathrm{in\ situ}}$ tends to be highly correlated with the halo mass. It is therefore unsurprising that we see a similar increase in orbital radii with increasing in situ stellar mass as with increasing M_{200c}.

We also considered other host parameters, including accreted stellar mass, in situ star formation time-scale (as a proxy for disc formation time), the stellar mass of the largest satellite, and the recent accretion rate of the host galaxy.[5] When normalizing orbits by viral radius R_{200c} in order to remove the effects of correlation with increasing halo mass and size, we find no clear trends with any of these properties. A host property that we have not been able to explore in this work is the presence of a nearby massive galaxy like M31. As discussed in Section 2, the Auriga galaxies are selected to be isolated systems due to computational limitations. Future studies of paired MW and M31-like systems will be necessary to understand the impact of environment on the population of disrupting satellites around the MW.

Further studies are called for to understand the significance of the trends highlighted in Fig. 10 and to investigate trends with other host galaxy and halo properties. Dropulic et al. (2024) study the effect of disrupting satellite orbits on host properties in semi-analytic models and identify similar trends with halo mass, disc mass, and disc density. Studies of the effect of host properties on disruption satellite populations are important while we are limited to a single observed galaxy (the MW). They will also be essential as we extend these analyses to external galaxies with upcoming observations from facilities such as Euclid (Racca et al. 2016), the Vera C. Rubin Observatory (Ivezić et al. 2019), the *Nancy Grace Roman Space Telescope* (Spergel et al. 2013), as well as from the ESA-selected ARRAKIHS[6] mission.

4 DISCUSSION AND CONCLUSION

In summary, we find that satellites around MW-mass galaxies in the Auriga simulations are highly disrupted, with the majority of 'surviving' satellites being classified as stellar streams (i.e. they have extended, coherent tidal tails). We also find that the subset of the satellite population that remains fully intact to $z = 0$ are recently accreted ($n_{\mathrm{peri}} \lesssim 1$) and have large pericentres ($r_{\mathrm{peri}} \gtrsim 50\,\mathrm{kpc}$) and apocentres ($r_{\mathrm{apo}} \gtrsim 200\,\mathrm{kpc}$). The disrupted satellites, however, span a much larger range of accretion times, pericentres, and apocentres. There is a strong apparent discrepancy in both the number and the orbits of the fully intact satellites in the Auriga simulations and those observed around the MW. There are more known MW satellites (in the resolved mass range) than the number of *intact* satellites in any Auriga simulation, and the orbits of the surviving MW satellites overlap significantly with both the intact and disrupting satellite population in Auriga. This apparent discrepancy may be resolved

---

[5] We define the recent mass accretion rate of the host between $z = 0 - 0.5$ as $\Gamma \equiv \Delta \log(M_{200c})/\Delta \log(a)$, from Diemer & Kravtsov (2014).
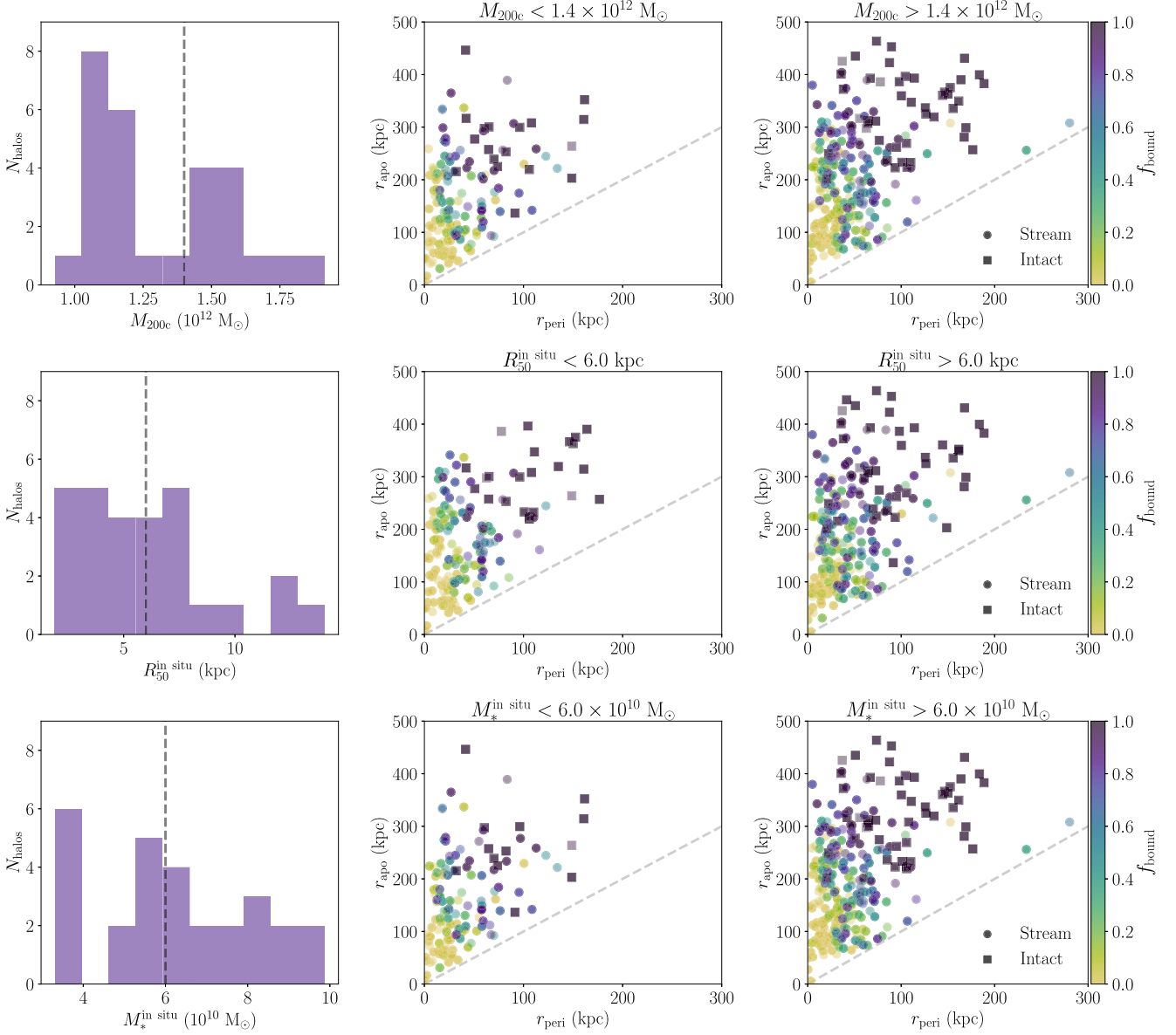[6] ARRAKIHS Phase 2 Proposal (public, pdf)

Figure 10. Pericentres and apocentres of intact satellites and stellar streams around 28 level 4 host galaxies binned by host galaxy properties. In the top row, galaxies are binned by host halo mass (M_{200c}). The histogram on the left shows the distribution of host masses across the 28 simulations and the grey dashed line indicates that value on which the sample is split. The panels in the centre and right show the pericentres and apocentres of satellites around galaxies in each mass bin. The middle row shows the same for disc size ($R_{50}^{\rm in\ situ}$, defined as the spherical radius which encloses 50 per cent of in situ stellar mass), and the bottom row shows the distribution across host in situ stellar mass ($M_*^{\rm in\ situ}$).

if the MW satellites are in fact *more highly disrupted* than has previously been observed. This higher disruption rate may also help us to explain recent observations of extratidal stars around MW satellite galaxies, including those with large pericentric distances (e.g. Jensen et al. 2024).

In the future, we will generate mock-observed catalogues of resolved stellar populations in the simulated satellites and compare to detectable satellites and tidal tails in the MW in order to determine whether this predicted high disruption rate of MW satellites is in fact consistent with current observations.

Another key finding is that many of the Auriga simulations have stellar streams on orbits consistent with the MW dwarf galaxy streams ($r_{\rm peri} \lesssim 20\,{\rm kpc}$, $r_{\rm apo} \lesssim 50\,{\rm kpc}$). This is different from the findings of Shipp et al. (2023) using FIRE-2 simulations. However,

among the larger sample of 28 Auriga simulations, we find significant halo-to-halo variance (a conclusion also supported by semi-analytic models in Dropulic et al. 2024), with some Auriga simulations more similar to the MW distribution, and some more similar to FIRE-2. Therefore, given the relatively small sample size (28 galaxies in Auriga, 13 in FIRE-2), it is difficult to tell whether any observed differences in orbital properties are due to the effect of halo-to-halo variance or in fact due to model-based differences. It is possible that the 13 FIRE-2 galaxies studied in Shipp et al. (2023) just happened to be systems with streams orbiting at larger distances from the centre of the host galaxy.

If these 13 galaxies are in fact representative of all FIRE-2 galaxies, the lack of streams at small pericentres and apocentres could be due to a higher rate of phase-mixing in the inner galaxy (e.g. due to

more time-dependence in the central potential) than in the Auriga simulations. It does not appear that the difference lies in the initial satellite disruption rates, because the orbits of the intact satellite population appear to be consistent between the simulations – there is only a difference in whether certain disrupting satellites in the inner galaxy are classified as coherent stellar streams or phase-mixed systems. Interestingly, Santistevan et al. (2023) found that the orbits of surviving satellites in FIRE-2 tend to increase over time, possibly due to time-evolution of the host galaxy potential. This effect could also cause the streams to orbit at larger radii at $z = 0$. Importantly, both Auriga and FIRE form massive central discs, so purely the presence of a host galaxy is likely not driving the differences between these simulations and the observations.

On the other hand, we find a correlation between stream orbits and host halo mass (also supported by Dropulic et al. 2024), with less massive host galaxies having streams with smaller pericentres and apocentres. If the MW's halo mass is less than 10^{12} M$_\odot$, as suggested by some recent measurements (e.g. Vasiliev et al. 2021; Koposov et al. 2023; Ou et al. 2024a, though see Oman & Riley 2024), we would expect the streams to be orbiting at smaller distances than predicted by either the FIRE-2 or Auriga simulations, which include host galaxies with masses of $1 - 2 \times 10^{12}$ M$_\odot$. These results call for studies of large numbers of stream populations with a range of host galaxy properties in both cosmological simulations and in semi-analytic models.

4.1 Simulation effects

Overall, the Auriga and FIRE-2 simulations predict very similar orbital distributions of disrupting satellites. In both simulations, the majority of satellites are disrupted and even the 'surviving' satellites have extended tidal tails and would be classified as stellar streams given perfect observations. There may be a difference in the orbits or phase-mixing rates of streams at small pericentres and apocentres, but as discussed above, this may be due solely to small sample sizes and the effect of halo-to-halo variance. If the disruption rates in these simulations are correct, the lack of observed tidal tails around Milky Way satellites could be due to their low surface brightness, a scenario verified for FIRE-2 (Shipp et al. 2023) but not yet for Auriga. The agreement between these distinct simulations strengthens the confidence in each of their predictions. This agreement is especially interesting given the differences between these sets of simulations.

One notable difference lies in the treatment of feedback processes and baryonic physics. The FIRE-2 simulations include detailed models of supernovae and stellar winds, attempting to directly capture these feedback processes (see the complete description in Hopkins et al. 2018; Wetzel et al. 2023). In contrast, Auriga adopts an effective feedback model, where isotropic winds are launched stochastically from supernova sites and are initially decoupled from the gas hydrodynamically until the wind particle enters a predetermined threshold density (at scales larger than star forming regions; see Grand et al. 2017). Additionally, the two simulations differ in their treatment of the interstellar medium. Auriga employs an effective model for the multiphase gas down to 10^4 K, while FIRE-2 aims to resolve individual gas phases and include low-temperature cooling down to 10 K. Despite these different methods, the gas mass resolution remains comparable between FIRE-2 and Auriga level 3 (Wetzel et al. 2016; Grand et al. 2017). Finally, the two simulations use different gravitational solvers and softening parameters, including variations in the softening lengths (Springel 2010; Hopkins 2015; Wetzel et al. 2016; Grand et al. 2017, 2024). These modelling choices may lead to discrepancies in the structure and time evolution of both satellites

and host galaxies, which could affect disruption rates. However, given the subtleties and complexities of these models, the specific impact of these differences on satellite dynamics requires further targeted investigation. Purely numerical effects could also be tested through comparison projects like AGORA, which examine the influence of simulation techniques on satellite evolution (Kim et al. 2014; Jung et al. 2024).

On the other hand, both the Auriga and FIRE-2 simulations are susceptible to certain numerical issues. These challenges are particularly evident in the number of particles used to sample the dark matter and stellar distribution functions of the satellites, as well as in potential discrepancies with particle mass ratios. Tailored N-body simulations (van den Bosch & Ogiya 2018; Errani & Peñarrubia 2020; Errani & Navarro 2021; Green, van den Bosch & Jiang 2021) have demonstrated lower subhalo disruption rates, suggesting that satellites may disrupt artificially when the particle count or force resolution is insufficient. However, these controlled experiments do not fully replicate the complexities of a cosmological environment, such as satellite pre-processing or the effects of a central massive disc and time-evolving potential, which are crucial for accurately modelling satellite evolution (Garrison-Kimmel et al. 2017; Kelley et al. 2019; He et al. 2025; Wang et al. 2025).[7] Spurious heating due to unequal dark matter and star particle masses or insufficient particle number could also cause the satellites to disrupt more quickly than they should (see Ludlow et al. 2019, 2020, 2021, 2023). However, this effect has not been thoroughly tested for satellite systems (as opposed to central galaxies), and further study is needed, likely involving high-resolution simulations and convergence tests across different simulation suites.

4.2 Implications for Milky Way satellites

If the disruption rates predicted by cosmological simulations like Auriga are indeed correct, then the MW satellites are likely much more disrupted than we have yet to observe. This is not necessarily inconsistent with current observations, given that the tidal tails tend to be quite diffuse and low surface brightness, and in many cases the surviving bound components of the galaxies remain relatively undisturbed.

Future observations may reveal evidence of tidal disruption around existing satellites. In particular, deep photometric observations with surveys like the Rubin Observatory Legacy Survey of Space and Time (LSST; LSST Science Collaboration 2009) are well-suited to reveal low surface brightness stellar density features like stellar streams (Ivezić et al. 2019). Narrow band photometric surveys targeting metallicity-sensitive lines such as CaHK (e.g. Starkenburg et al. 2017) are also powerful tools in selecting the metal-poor member stars of known satellites across larger areas. Proper motions from *Gaia* have been used to select member stars out to larger distances around known satellites, as in Jensen et al. (2024), and future *Gaia* data releases will provide even higher precision proper motion measurements that may enable improved selection of member stars beyond the tidal radii of these satellites. Finally, wide-field spectroscopic surveys such as the Dark Energy Spectroscopic Instrument (DESI; Cooper et al. 2023; Koposov et al. 2024), 4MOST (de Jong et al. 2019), and WEAVE (Dalton 2016) will also facilitate the identification of members across a wider area than more targeted spectroscopic observations. Furthermore, when taken

---

[7]For further discussions of numerical tests of these effects in a cosmological context, see Grand et al. (2021); Barry et al. (2023); Donlon et al. (2024).

together, these surveys will provide full kinematic measurements of a large sample of member stars of these satellites, enabling dynamical models that may be used to reveal the disruption history of the MW satellite population. Future work will consider the disrupting satellites in Auriga in the context of the MW and make predictions for observational measurements that may be used to further test the predictions of these simulations in comparison to the MW satellite population. Finally, future observations with LSST, Euclid (Racca et al. 2016), the *Nancy Grace Roman Space telescope* (Spergel et al. 2013), and the ESA-selected ARRAKHHIS mission will also reveal populations of satellites and stellar streams around MW-mass hosts external to our own galaxy, thereby providing a larger sample size with which to compare our simulations.

High stellar disruption rates also have implications for the dark matter components of the MW satellite galaxies. The majority of the dark matter is stripped before these systems begin losing stars, so satellites that have experienced the level of stellar disruption that we see in Auriga would have very low-mass dark matter components. This could bias dwarf galaxy mass modelling measurements and dark matter indirect detection constraints, though constraints based on comparisons to cosmological simulations would already incorporate these effects (e.g. Wang et al. 2022; Vienneau et al. 2024). The detailed dark matter distributions of the Auriga satellites and the resulting effect on dark matter constraints using MW satellites will be examined in future work.

As discussed above, there are many assumptions and approximations that go into these complex simulations that could potentially lead to artificially high tidal disruption rates of the Auriga satellite population. If instead, the Auriga and FIRE-2 simulations are overdisrupting satellites, the results presented here still have important implications for studies of the MW satellite population in the context of predictions of ΛCDM and galaxy formation models. Many suites of hydrodynamic cosmological simulations, including Auriga, do an excellent job of reproducing many properties of the surviving satellite population as observed around the MW. However, if these satellites are in fact over-disrupted, then there must be significant remaining discrepancies, including in the total mass function of satellites (the total masses of Auriga satellites are higher than their present day masses given the significant tidal mass-loss), the structures of satellite galaxies (density profiles of satellites affect disruption rates), and the orbits of satellites and their radial distributions within the MW. These discrepancies would indicate significant remaining gaps in our understanding of small-scale galaxy formation in the context of ΛCDM. Truly understanding whether our simulations of satellite galaxy populations in ΛCDM are able to reproduce MW observations will require a more thorough understanding of disruption rates of satellite galaxies in both simulations and in observations.

ACKNOWLEDGEMENTS

DATA AVAILABILITY

Halo catalogues, merger trees, and particle data (Section 2) for Auriga levels 3 and 4 are publicly available (detailed in the Auriga project data release; Grand et al. 2024) to download via the Globus plat-

form.[8] Auriga level 2 data products will be shared upon reasonable request. The orbits and properties of the disrupting satellite galaxies characterized in this article (Section 3) are available in Appendix A and on the Auriga webpage.

REFERENCES

Arora A. et al., 2024, ApJ, 977, 23

Arora A., Sanderson R. E., Panithanpaisal N., Cunningham E. C., Wetzel A., Garavito-Camargo N., 2022, ApJ, 939, 2

Astropy Collaboration 2013, A&A, 558, A33

Astropy Collaboration 2018, AJ, 156, 123

Astropy Collaboration 2022, ApJ, 935, 167

Barry M., Wetzel A., Chapman S., Samuel J., Sanderson R., Arora A., 2023, MNRAS, 523, 428

Behnel S., Bradshaw R., Citro C., Dalcin L., Seljebotn D. S., Smith K., 2011, Comput. Sci. Eng., 13, 31

Belokurov V. et al., 2006, ApJ, 642, L137

Belokurov V., Erkal D., Evans N. W., Koposov S. E., Deason A. J., 2018, MNRAS, 478, 611

Bernard E. J. et al., 2016, MNRAS, 463, 1759

Bonaca Ana, Price-Whelan Adrian M., 2025, New Astron. Rev., 100, 101713

Bose S., Deason A. J., Belokurov V., Frenk C. S., 2020, MNRAS, 495, 743

Brooks A. M., Zolotov A., 2014, ApJ, 786, 87

Brooks R.A.N., Garavito-Camargo N., Johnston K.V., Price-Whelan A.M., Sanders J.L., Lilleengen S., 2024, ApJ, 978, 79

Buitinck L. et al., 2013, in ECML PKDD Workshop: Languages for Data Mining and Machine Learning. p. 108

Bullock J. S., Boylan-Kolchin M., 2017, ARA&A, 55, 343

Bullock J. S., Johnston K. V., 2005, ApJ, 635, 931

Callingham T. M. et al., 2019, MNRAS, 484, 5453

Carlin J. L., Sand D. J., 2018, ApJ, 865, 7

Chiti A. et al., 2021, Nat. Astron., 5, 392

Collette A. et al., 2022, h5py/h5py: 3.7.0, Zenodo. Available at: https://doi.org/10.5281/zenodo.6575970

Collette A., 2013, Python and HDF5. O'Reilly, Sebastopol,CA. Available at: https://www.oreilly.com/library/view/python-and-hdf5/9781491944981/

Cooper A. P. et al., 2023, ApJ, 947, 37

D'Souza R., Bell E. F., 2022, MNRAS, 512, 739

Dalton G., 2016, in Skillen I., Balcells M., Trager S., eds, ASP Conf. Ser. Vol. 507, Multi-Object Spectroscopy in the Next Decade: Big Questions, Large Surveys, and Wide Fields. Astron. Soc. Pac., San Francisco, p. 97

Davis M., Efstathiou G., Frenk C. S., White S. D. M., 1985, ApJ, 292, 371

de Jong R. S. et al., 2019, The Messenger, 175, 3

Deason A. J., Belokurov V., Koposov S. E., Gómez F. A., Grand R. J., Marinacci F., Pakmor R., 2017, MNRAS, 470, 1259

Deason A. J., Bose S., Fattahi A., Amorisco N. C., Hellwing W., Frenk C. S., 2022, MNRAS, 511, 4044

Deason A. J., Fattahi A., Belokurov V., Evans N. W., Grand R. J. J., Marinacci F., Pakmor R., 2019, MNRAS, 485, 3514

DES Collaboration, 2016, MNRAS, 460, 1270

Diemer B., Kravtsov A. V., 2014, ApJ, 789, 1

Donlon T., Newberg H. J., Sanderson R., Bregou E., Horta D., Arora A., Panithanpaisal N., 2024, MNRAS, 531, 1422

Drlica-Wagner A. et al., 2020, ApJ, 893, 47

Drlica-Wagner A. et al., 2021, ApJS, 256, 2

Dropulic A., Shipp N., Kim S., Mezghanni Z., Necib L., Lisanti M., 2024, preprint (arXiv:2409.13810)

Erkal D. et al., 2018, MNRAS, 481, 3148

Erkal D. et al., 2019, MNRAS, 487, 2685

Errani R., Navarro J. F., 2021, MNRAS, 505, 18

Errani R., Peñarrubia J., 2020, MNRAS, 491, 4591

Errani R., Peñarrubia J., Laporte C. F. P., Gómez F. A., 2017, MNRAS, 465, L59

Fattahi A. et al., 2019, MNRAS, 484, 4471

Fattahi A. et al., 2020, MNRAS, 497, 4459

Fattahi A., Navarro J. F., Frenk C. S., Oman K. A., Sawala T., Schaller M., 2018, MNRAS, 476, 3816

Faucher-Giguère C.-A., Lidz A., Zaldarriaga M., Hernquist L., 2009, ApJ, 703, 1416

Filion C., Wyse R. F. G., 2021, ApJ, 923, 218

Garavito-Camargo N., Besla G., Laporte C. F. P., Price-Whelan A. M., Cunningham E. C., Johnston K. V., Weinberg M., Gómez F. A., 2021, ApJ, 919, 109

Garrison-Kimmel S. et al., 2017, MNRAS, 471, 1709

Garrison-Kimmel S., Hopkins P. F, Wetzel A., Bullock J. S, Boylan-Kolchin M., Kereš D., Faucher-Giguère C.-A., El-Badry K., Lamberts A., Quataert E., Sanderson R., 2019. MNRAS, 487, 1380

Gómez F. A., Besla G., Carpintero D. D., Villalobos Á., O'Shea B. W., Bell E. F., 2015, ApJ, 802, 128

Gómez F. A., Helmi A., Cooper A. P., Frenk C. S., Navarro J. F., White S. D. M., 2013, MNRAS, 436, 3602

Gómez F. A., White S. D. M., Marinacci F., Slater C. T., Grand R. J. J., Springel V., Pakmor R., 2016, MNRAS, 456, 2779

Gommers R. et al., 2022, scipy/scipy: SciPy 1.9.1, Zenodo. Available at: https://doi.org/10.5281/zenodo.7026742

Grand R. J. J. et al., 2017, MNRAS, 467, 179

Grand R. J. J. et al., 2021, MNRAS, 507, 4953

Grand R. J. J., Fragkoudi F., Gómez F. A., Jenkins A., Marinacci F., Pakmor R., Springel V., 2024, MNRAS, 532, 1814

Green S. B., van den Bosch F. C., Jiang F., 2021, MNRAS, 503, 4075

Grillmair C. J., 2006, ApJ, 645, L37

Grisel O. et al., 2022, scikit-learn/scikit-learn: scikit-learn 1.1.2, Zenodo. Available at: https://doi.org/10.5281/zenodo.6968622

Harris C. R. et al., 2020, Nature, 585, 357

He F., Han J., Li Z., 2025, ApJ, 981, 108

Helmi A., Babusiaux C., Koppelman H. H., Massari D., Veljanoski J., Brown A. G. A., 2018, Nature, 563, 85

Hopkins P. F. et al., 2018, MNRAS, 480, 800

Hopkins P. F., 2015, MNRAS, 450, 53

Hunter J. D., 2007, Comput. Sci. Eng., 9, 90

Ivezić Ž. et al., 2019, ApJ, 873, 111

Jenkins A., 2013, MNRAS, 434, 2094

Jensen J., Hayes C. R., Sestito F., McConnachie A. W., Waller F., Smith S. E. T., Navarro J., Venn K. A., 2024, MNRAS, 527, 4209

Ji A.P., et al., 2021. ApJ, 921, 32

Jung M. et al., 2024, ApJ, 964, 123

Kallivayalil N. et al., 2018, ApJ, 867, 19

Kelley T., Bullock J. S., Garrison-Kimmel S., Boylan-Kolchin M., Pawlowski M. S., Graus A. S., 2019, MNRAS, 487, 4409

Khoperskov S. et al., 2023, A&A, 677, A90

Kim J.-h. et al., 2014, ApJS, 210, 14

Kluyver T. et al., 2016, in Loizides F., Scmidt B., eds, Positioning and Power in Academic Publishing: Players, Agents and Agendas. IOS Press, the Netherlands, p. 87

Koposov S. E. et al., 2019, MNRAS, 485, 4726

Koposov S. E. et al., 2023, MNRAS, 521, 4936

Koposov S. E. et al., 2024, MNRAS, 533, 1012

Koposov S. E., Irwin M., Belokurov V., Gonzalez-Solares E., Yoldas A. K., Lewis J., Metcalfe N., Shanks T., 2014, MNRAS, 442, L85

Li T. S. et al., 2021, ApJ, 911, 149

Li T. S. et al., 2022, ApJ, 928, 30

Li Y.-S., Helmi A., 2008, MNRAS, 385, 1365

Lilleengen S. et al., 2023, MNRAS, 518, 774

LSST Science Collaboration, 2009, preprint (arXiv:0912.0201)

Ludlow A. D., Fall S. M., Schaye J., Obreschkow D., 2021, MNRAS, 508, 5114

Ludlow A. D., Fall S. M., Wilkinson M. J., Schaye J., Obreschkow D., 2023, MNRAS, 525, 5614

Ludlow A. D., Schaye J., Schaller M., Bower R., 2020, MNRAS, 493, 2926

[8]https://wwwmpa.mpa-garching.mpg.de/auriga/data

Ludlow A. D., Schaye J., Schaller M., Richings J., 2019, MNRAS, 488, L123
Malhan K., Ibata R. A., 2018, MNRAS, 477, 4063
Marinacci F., Grand R. J. J., Pakmor R., Springel V., Gómez F. A., Frenk C. S., White S. D. M., 2017, MNRAS, 466, 3859
Marinacci F., Pakmor R., Springel V., 2014, MNRAS, 437, 1750
Mateu C., 2023, MNRAS, 520, 5225
McKinney W., 2010, in van der Walt S., Millman J., eds, Proceedings of the 9th Python in Science Conference. SciPy, Austin,Texas, p. 56
Monachesi A. et al., 2019, MNRAS, 485, 2589
Monachesi A., Gómez F. A., Grand R. J. J., Kauffmann G., Marinacci F., Pakmor R., Springel V., Frenk C. S., 2016, MNRAS, 459, L46
Mori A., Di Matteo P., Salvadori S., Khoperskov S., Pagnini G., Haywood M., 2024, A&A, 690, A136
Munshi F., Brooks A. M., Applebaum E., Christensen C. R., Quinn T., Sligh S., 2021, ApJ, 923, 35
Nadler E. O. et al., 2020, ApJ, 893, 48
Nadler E. O., Birrer S., Gilman D., Wechsler R. H., Du X., Benson A., Nierenberg A. M., Treu T., 2021, ApJ, 917, 7
Nadler E. O., Mao Y.-Y., Wechsler R. H., Garrison-Kimmel S., Wetzel A., 2018, ApJ, 859, 129
Naidu R. P., Conroy C., Bonaca A., Johnson B. D., Ting Y.-S., Caldwell N., Zaritsky D., Cargile P. A., 2020, ApJ, 901, 48
Oman K. A., Riley A. H., 2024, MNRAS, 532, L48
Ou X. et al., 2024b, ApJ, 966, 33
Ou X., Eilers A.-C., Necib L., Frebel A., 2024a, MNRAS, 528, 693
Pace A. B., Erkal D., Li T.S., 2022, ApJ, 940, 136
Pakmor R. et al., 2017, MNRAS, 469, 3185
Pakmor R., Springel V., Bauer A., Mocz P., Munoz D. J., Ohlmann S. T., Schaal K., Zhu C., 2016, MNRAS, 455, 1134
pandas development team T., 2022, pandas-dev/pandas: Pandas, Zenodo, https://doi.org/10.5281/zenodo.7093122
Panithanpaisal N., Sanderson R. E., Wetzel A., Cunningham E. C., Bailin J., Faucher-Giguère C.-A., 2021, ApJ, 920, 10
Patel E. et al., 2020, ApJ, 893, 121
Pedregosa F. et al., 2011, J. Mach. Learn. Res., 12, 2825
Perez F., Granger B. E., 2007, Comput. Sci. Eng., 9, 21
Planck Collaboration XVI 2014, A&A, 571, A16
Pozo A., Broadhurst T., de Martino I., Chiueh T., Smoot G. F., Bonoli S., Angulo R., 2024, Phys. Rev. D, 110, 043534
Qi Y., Zivick P., Pace A. B., Riley A. H., Strigari L. E., 2022, MNRAS, 512, 5601
Racca G. D. et al., 2016, in MacEwen H. A., Fazio G. G., Lystrup M., Batalha N., Siegler N., Tong E. C., eds, Proc. SPIE Conf. Ser. Vol. 9904, Space Telescopes and Instrumentation 2016: Optical, Infrared, and Millimeter Wave. SPIE, Bellingham, p. 99040O
Revaz Y., Jablonka P., 2018, A&A, 616, A96
Richings J. et al., 2020, MNRAS, 492, 5780
Riley A. H. et al., 2019, MNRAS, 486, 2679
Riley A.~H., Shipp N., Simpson C.~M., Bieri R., Fattahi A., Brown S.~T., Oman K.~A., et al., 2024, preprint( )
Rocha M., Peter A. H. G., Bullock J., 2012, MNRAS, 425, 231
Sales L. V., Wetzel A., Fattahi A., 2022, Nat. Astron., 6, 897
Samuel J. et al., 2020, MNRAS, 491, 1471
Sanders J. L., Lilley E. J., Vasiliev E., Evans N. W., Erkal D., 2020, MNRAS, 499, 4793
Santistevan I. B., Wetzel A., Tollerud E., Sanderson R. E., Moreno J., Patel E., 2024, MNRAS, 527, 8841
Santistevan I. B., Wetzel A., Tollerud E., Sanderson R. E., Samuel J., 2023, MNRAS, 518, 1427
Santos-Santos I. M. E., Fattahi A., Sales L. V., Navarro J. F., 2021, MNRAS, 504, 4551
Sawala T. et al., 2016, MNRAS, 457, 1931
Schaye J. et al., 2015, MNRAS, 446, 521
Searle L., Zinn R., 1978, ApJ, 225, 357
Sestito F. et al., 2023, MNRAS, 525, 2875
Shipp N. et al., 2018, ApJ, 862, 114
Shipp N. et al., 2021, ApJ, 923, 149
Shipp N. et al., 2023, ApJ, 949, 44
Simpson C. M., Grand R. J. J., Gómez F. A., Marinacci F., Pakmor R., Springel V., Campbell D. J. R., Frenk C. S., 2018, MNRAS, 478, 548
Spergel D. et al., 2013, preprint (arXiv:1305.5422)
Springel V., 2005, MNRAS, 364, 1105
Springel V., 2010, MNRAS, 401, 791
Springel V., Di Matteo T., Hernquist L., 2005, MNRAS, 361, 776
Springel V., Hernquist L., 2003, MNRAS, 339, 289
Springel V., White S. D. M., Tormen G., Kauffmann G., 2001, MNRAS, 328, 726
Starkenburg E. et al., 2017, MNRAS, 471, 2587
Tarumi Y., Yoshida N., Frebel A., 2021, ApJ, 914, L10
Torrealba G. et al., 2019, MNRAS, 488, 2743
van den Bosch F. C., Ogiya G., 2018, MNRAS, 475, 4066
van der Velden E., 2020, J. Open Source Softw., 5, 2004
van der Velden E., Robert C., Batten A., Clauss C., beskep (Daniel) H., Thyng K., 2024, 1313e/CMasher: v1.8.0, Zenodo. Available at: https://doi.org/10.5281/zenodo.10677366
Vasiliev E., 2019, MNRAS, 482, 1525
Vasiliev E., 2024, MNRAS, 527, 437
Vasiliev E., Belokurov V., Erkal D., 2021, MNRAS, 501, 2279
Vera-Casanova A. et al., 2022, MNRAS, 514, 4898
Vienneau E., Evans A.J., Hartl O.V., Bozorgnia N., Strigari L.E., Riley A.H., Shipp N., 2024. J. Cosmol. Astropart. Phys., 2024, 019
Virtanen P. et al., 2020, Nat. Methods, 17, 261
Vivas A. K., Martínez-Vázquez C. E., Walker A. R., Belokurov V., Li T. S., Erkal D., 2022, ApJ, 926, 78
Vogelsberger M., Genel S., Sijacki D., Torrey P., Springel V., Hernquist L., 2013, MNRAS, 436, 3031
Wagg T., Broekgaarden F. S., 2024, preprint (arXiv:2406.04405)
Wagg T., Broekgaarden F., Gültekin K., 2024, TomWagg/software-citation-station: v1.2, Zenodo. Available at: https://doi.org/10.5281/zenodo.13225824
Wang W. et al., 2022, ApJ, 941, 108
Wang W., Han J., Cautun M., Li Z., Ishigaki M. N., 2020, Sci. China Phys. Mech. Astron., 63, 109801
Wang Y., Mansfield P., Nadler E.O., Darragh-Ford E., Wechsler R. H., Yang D., Yu H.-B., 2025. ApJ, 986, 147
Wetzel A. et al., 2023, ApJS, 265, 44
Wetzel A. R., Deason A. J., Garrison-Kimmel S., 2015, ApJ, 807, 49
Wetzel A. R., Hopkins P. F., Kim J.-h., Faucher-Giguère C.-A., Kereš D., Quataert E., 2016, ApJ, 827, L23
York D. G. et al., 2000, AJ, 120, 1579

SUPPORTING INFORMATION

Supplementary data are available at *MNRAS* online.

suppl_data

Please note: Oxford University Press is not responsible for the content or functionality of any supporting materials supplied by the authors. Any queries (other than missing material) should be directed to the corresponding author for the article.

APPENDIX A: CATALOGUE OF ACCRETED STRUCTURES

In Table A1 we present the complete catalogue of accretion events identified in Paper I, in addition to orbital properties determined in this work (Section 3.1). The system IDs match the 'accreted particle lists' in the Auriga public data release (Grand et al. 2024).

Table A1. Catalogue of accretion events and their properties analysed in this work, sorted by level, then halo number, then stellar mass. For brevity, we only show systems for the level 3 run of Au-6 in this paper. We provide the halo number, resolution level, and system ID that in combination uniquely identify an object (IDs alone are not guaranteed to be unique); morphological classification; total stellar mass (M_*), including bound progenitor if still present at $z = 0$; fraction of stellar mass bound to the progenitor (f_{bound}); pericentre (r_{peri}); apocentre (r_{apo}); accretion time (t_{acc}) defined as first crossing of the host's R_{200c}; distance from the host at the present day for accretions with a bound progenitor; and the matched ID of the same object at one resolution level higher. A machine-readable table with the full catalogue is available as supplementary material.

Halo	Level	ID	Morphology	$\log_{10}(M_*/M_\odot)$	f_{bound}	r_{peri} (kpc)	r_{apo} (kpc)	t_{acc} (Gyr)	Distance (kpc)	Preprocessed	Match ID
						. . .					
6	3	176	intact	9.54	0.997	152.99	–	1.94	199.79	False	232
6	3	22562	phase-mixed	9.43	0.000	0.00	0.05	11.05	–	False	433688
6	3	144	phase-mixed	9.05	0.000	0.01	0.39	9.22	–	False	102240
6	3	2518	phase-mixed	9.04	0.000	0.01	0.79	8.90	–	False	91904
6	3	2333	phase-mixed	9.00	0.000	0.85	24.42	8.90	–	False	3612
6	3	151	phase-mixed	8.96	0.000	0.03	2.59	8.60	–	False	184
6	3	92	phase-mixed	8.78	0.000	0.01	0.39	9.52	–	False	91897
6	3	175	intact	8.40	0.990	73.79	225.01	6.07	129.62	False	231
6	3	40792	phase-mixed	8.38	0.000	0.00	0.08	11.66	–	False	660895
6	3	2763	stream	7.97	0.410	15.87	165.67	6.40	37.60	False	3372
6	3	2729	stream	7.73	0.001	27.64	55.02	8.90	44.65	False	102455
6	3	13801	phase-mixed	7.42	0.000	0.02	1.20	9.22	–	False	–
6	3	40886	phase-mixed	7.24	0.000	0.03	4.98	11.66	–	False	484645
6	3	33060	phase-mixed	7.16	0.000	11.64	97.19	8.60	–	True	403733
6	3	365	intact	7.03	0.998	57.14	–	2.25	217.36	False	3105
6	3	13857	stream	6.98	0.134	22.41	99.02	10.75	35.11	False	392843
6	3	82	phase-mixed	6.96	0.000	0.95	14.15	11.93	–	False	151
6	3	450129	phase-mixed	6.93	0.000	0.04	1.54	12.18	–	False	1346443
6	3	441235	phase-mixed	6.81	0.000	0.01	1.04	11.66	–	False	1375567
6	3	1022	stream	6.80	0.544	18.15	334.69	8.28	197.17	True	7306
6	3	40713	phase-mixed	6.78	0.000	15.91	59.88	11.36	–	False	608072
6	3	86344	stream	6.70	0.000	26.24	156.81	8.60	–	True	423599
6	3	54423	intact	6.52	1.000	–	–	–	270.26	False	8695
6	3	4317	stream	6.49	0.921	26.87	364.90	7.99	97.46	False	96349
6	3	439497	stream	6.47	0.097	–	57.75	11.36	32.36	False	608129
6	3	66116	phase-mixed	6.46	0.000	0.34	15.55	11.66	–	False	1969087
6	3	86785	phase-mixed	6.45	0.000	0.52	17.84	8.60	–	True	510516
6	3	450183	phase-mixed	6.42	0.000	0.17	5.46	12.56	–	False	1346695
6	3	60914	phase-mixed	6.41	0.000	0.23	4.67	12.18	–	False	834323
6	3	450996	phase-mixed	6.40	0.000	0.12	2.70	12.56	–	False	1346807
6	3	820096	phase-mixed	6.35	0.000	0.06	3.10	11.93	–	False	661067
6	3	119824	stream	6.21	0.000	10.94	169.01	8.90	–	True	510560
6	3	401238	phase-mixed	6.19	0.000	0.95	38.04	8.90	–	True	485312
6	3	818755	phase-mixed	6.15	0.000	18.64	47.26	11.36	–	False	786494
6	3	22636	phase-mixed	6.14	0.000	1.51	20.92	11.05	–	False	709923
6	3	83559	phase-mixed	6.09	0.000	29.49	117.54	9.52	–	True	485601
6	3	820255	phase-mixed	6.07	0.000	1.47	9.01	11.93	–	False	7675517
6	3	86573	phase-mixed	6.00	0.000	1.48	29.02	8.60	–	True	510832
6	3	98912	stream	5.98	0.525	25.77	235.18	10.13	206.71	False	423105
6	3	22641	stream	5.96	0.000	100.50	229.46	11.05	–	False	480459
6	3	105073	intact	5.96	0.978	60.45	297.28	6.07	177.53	False	527547
6	3	451182	phase-mixed	5.94	0.000	0.04	1.17	12.56	–	False	3975982
6	3	25426	stream	5.84	0.067	52.84	100.88	9.22	65.77	False	439605
6	3	450937	phase-mixed	5.83	0.000	0.59	9.11	12.56	–	False	1346868
6	3	466589	phase-mixed	5.80	0.000	0.34	6.34	12.56	–	False	3971198
6	3	461836	phase-mixed	5.74	0.000	0.00	0.51	13.07	–	False	4028766
6	3	441640	phase-mixed	5.71	0.000	0.03	4.03	11.66	–	False	661038
6	3	461788	phase-mixed	5.71	0.000	0.03	1.09	12.85	–	False	140
6	3	60987	phase-mixed	5.70	0.000	0.06	6.22	12.85	–	False	1735450
6	3	52829	phase-mixed	5.69	0.000	0.83	14.32	9.52	–	True	1719764
						. . .					

This paper has been typeset from a TEX/LATEX file prepared by the author.